An *ab initio* Molecular-orbital Study of Insertion of CO_2 into a Rh^I–H Bond†

Shigeyoshi Sakaki* and Yasuo Musashi
Department of Applied Chemistry, Faculty of Engineering, Kumamoto University, Kurokami, Kumamoto 860, Japan

The insertion of CO_2 into the Rh^I–H bond of $[RhH(PH_3)_3]$ was investigated theoretically by the *ab initio* molecular-orbital method, in which geometries of the reactants, the transition state and products were optimized at the Hartree–Fock level, and MP4SDQ, SDCI and coupled cluster calculations were carried out on those optimized structures. This reaction is calculated to occur with a higher activation energy (16 kcal mol^{-1}) and lower exothermicity (24 kcal mol^{-1}) than the similar insertion into the Cu^I–H bond of $[CuH(PH_3)_2]$ (E_a = 3.5 kcal mol^{-1} and E_{exo} = *ca.* 40 kcal mol^{-1}), calculated at the SDCI level. The lower exothermicity arises from the fact that the Rh^I–H bond is much stronger than the Cu^I–H bond. The higher activation energy is interpreted in terms of the stronger Rh^I–H bond, the weaker electrostatic stabilizing interaction and the stronger exchange repulsion interaction between CO_2 and $[RhH(PH_3)_3]$ in the transition state. Owing to this strong exchange repulsion, the transition state does not contain a four-centre type interaction.

Since insertion reactions of alkenes, alkynes and CO into M–H and M–R bonds (R = alkyl) are involved as key elementary processes in various catalytic cycles with transition-metal complexes,[1] the insertion of CO_2 into M–H and M–R bonds is believed to be of significant important in transition-metal catalysed conversion of CO_2 into useful chemicals.[2] In this context, detailed knowledge of the insertion reaction is necessary to understand the catalytic conversion and its further development. To obtain such knowledge, not only experimental work but also theoretical works should be carried out on the insertion. Theoretical work can offer meaningful information on the changes in geometry, transition state, bonding nature, electron distribution, activation energy, *etc.* However, only a few molecular-orbital (MO) studies have been reported on the insertion reactions of CO_2 into Cu^I–R (R = H or Me)[3] and Cr^0–H bonds.[4]

Besides these insertion reactions, that into the Rh–R bond (R = H, Me or Ph) is considered to be important because rhodium complexes are involved in various catalytic reactions.[1] So far several rhodium hydride and alkyl complexes have been reported to undergo insertion of CO_2. For instance, CO_2 reacts with $[RhPh(PR_3)_3]$ (R = Me or Ph) according to equation (1).[5]

$$[RhPh(PR_3)_3] + CO_2 \longrightarrow [Rh\{OC(O)Ph\}(PR_3)_3] \longrightarrow [Rh(O_2CPh)(PR_3)_2] + PR_3 \quad (1)$$

Similar insertions of CO_2 into Ru^I–H and Rh^{III}–H bonds are involved as key processes in catalytic hydrogenation of CO_2 to formic acid [equation (2)][6,7] [L–L = $Ph_2P(CH_2)_nPPh_2$, n = 2 or 3] and catalytic reduction of CO_2 to CO [equation (3) (R = Bu^t)][8] respectively. Also, the reverse of the insertion of CO_2 [equation (4), R = Ph] has been reported as a key

$$[RhH(L\text{–}L)_2] + CO_2 \longrightarrow [Rh(L\text{–}L)_2][HCO_2] \xrightarrow{H_2} [RhH(L\text{–}L)_2] + HCO_2H \quad (2)$$

$$[\overbrace{Rh(PR_2CH_2CH_2C_6H_3CH_2PR_2)H_2}] + CO_2 \longrightarrow [\overbrace{Rh(PR_2CH_2CH_2C_6H_3CH_2PR_2)H\{OC(O)H\}}] \longrightarrow [\overbrace{Rh(PR_2CH_2CH_2C_6H_3CH_2PR_2)H(OH)}] + CO \quad (3)$$

$$[Rh\{OC(O)H\}(PR_3)_3] \longrightarrow [RhH(PR_3)_3] + CO_2 \quad (4)$$

process of the decomposition of formic acid.[9] From these reactions we expect that rhodium complexes will serve as efficient catalysts for the conversion of CO_2 into useful chemicals. Thus, there is a considerable need to investigate theoretically the insertion of CO_2 into the Rh–R bond.

In the present work the insertion of CO_2 into the Rh^I–H bond of $[RhH(PH_3)_3]$ is investigated by *ab initio* MO/MP4, single and double excitation-configuration interaction (SDCI) and coupled cluster methods. This reaction is selected as a model of equations (1) and (4). Our purposes are (1) to obtain a detailed understanding of this insertion reaction, (2) to evaluate theoretically the activation energy and the energy of the reaction, and (3) to compare this insertion reaction with that into the Cu^I–H bond [equation (5)].[3] Through this

$$[CuH(PH_3)_2] + CO_2 \longrightarrow [Cu\{OC(O)H\}(PH_3)_2] \longrightarrow [Cu(O_2CH)(PH_3)_2] \quad (5)$$

investigation we hope to clarify differences between Cu^I and Rh^I in the insertion reaction.

Computational Details

Ab initio MO/MP4SDQ, SDCI and coupled cluster with double excitations (CCD) calculations were carried out by means of the GAUSSIAN 86[10] and 92[11] programs, using several kinds of basis sets. In basis set I the core electrons (up to 4p) of Rh were represented by Hay–Wadt's effective core potentials (ECP1), and valence orbitals (4d, 5s and 5p) by a (3s3p4d)/[2s2p2d] set.[12] For C and O, MIDI-3 sets were adopted,[13] while STO-2G was used for PH_3.[14] A (4s)/[2s] basis set[15] was employed for the active H atom which co-ordinates to Rh first and then reacts with CO_2. In basis set II the valence orbitals of Rh were represented by almost the same basis set (3s3p4d)/[2s2p3d] as before, and the ECP1 was used for core electrons (up to 4p) of Rh;[12] MIDI-4[13] sets were used for C, O

† *Non-SI units employed:* cal = 4.184 J, eV ≈ 1.60 × 10^{-19} J, E_h ≈ 4.36 × 10^{-18} J.

and P, and the (4s)/[2s] set[15] was employed for H. A p polarization (ζ = 1.0) was added[15] only for the active H atom. In basis set III core electrons (up to 3d) were represented by Hay–Wadt's effective core potentials (ECP2), and valence orbitals (4s, 4p, 4d, 5s and 5p) by a (5s5p4d)/[3s3p3d] set.[16] For H, C, O and P the same basis sets as those of II were adopted. In the basis set IV instead of ECP a (16s12p8d)/[6s5p4d] all-electron basis set was used for Rh,[13] where two p primitive functions[13] and one d primitive function [ζ = 0.08, determined according to the relation $\zeta_2 = (\zeta_1 \cdot \zeta_3)^{\frac{1}{2}}$, where the value decreases in the order $\zeta_1 > \zeta_2 > \zeta_3$] were added to represent valence 5p and 4d orbitals respectively. In basis set V, (9s5p)/[3s2p] sets were adopted for C and O,[16] while the same basis sets as those in IV were used for the other atoms.

The geometries of the reactants, transition state and products were optimized at the Hartree–Fock (HF) level with the energy-gradient technique, using basis set I,* where the geometry of PH_3 was taken to be the same as that in the experimental structure of the free molecule.†[18] The transition state was determined by evaluating the hessian matrix. The MP2-MP4SDQ, SDCI and CCD calculations were carried out with all core orbitals excluded from active space. In SDCI calculations, contributions from higher-order excited configurations were estimated, according to Davidson and Silver[20] and Pople *et al.*[21] In the CCD calculations the contributions of single and triple excitations were evaluated to fourth order using double-excitation wavefunctions. No instability of the HF wavefunctions[22] was observed for the reactants, transition state, and product.‡ However, the HF optimization followed by single-point MP4, CI, and CCD calculations would probably be invalid for several transition-metal systems. Since solvent effects were not considered, the present computations are meaningful for reactions in the gas phase or in non-polar solvents, *e.g.* several reactions of CO_2 with rhodium complexes have been carried out in benzene[5] and toluene.[8]

In order to investigate the bonding nature of the transition state we carried out an energy decomposition analysis according to Morokuma and co-workers.[23] In this analysis the interaction energy (INT) is defined as the stabilization energy of the reaction system relative to the reactants, CO_2 and $[RhH(PH_3)_3]$, taking distorted (dist) structures like that of the transition state (ts) [see equation (6)]. The

$$\mathrm{INT} = E_t[RhH(PH_3)_3 \cdots CO_2]_{ts} - E_t[RhH(PH_3)_3]_{dist} - E_t(CO_2)_{dist} \quad (6)$$

deformation energy (DEF) is defined as the destabilization energy which is necessary to distort CO_2 and $[RhH(PH_3)_3]$ from their equilibrium (eq) structures to the distorted ones in the transition state [see equation (7)]. The sum of INT and DEF

$$\mathrm{DEF} = E_t[RhH(PH_3)_3]_{dist} - E_t[RhH(PH_3)_3]_{eq} + E_t(CO_2)_{dist} - E_t(CO_2)_{eq} \quad (7)$$

corresponds to the activation energy (E_a) relative to the reactants [equation (8)]. The interaction energy is further divided into several chemically meaningful terms [equation (9)]:

$$E_a = \mathrm{INT} + \mathrm{DEF} = E_t[RhH(PH_3)_3 \cdots CO_2]_{ts} - E_t[RhH(PH_3)_3]_{eq} - E_t(CO_2)_{eq} \quad (8)$$

$$\mathrm{INT} = \mathrm{ES} + \mathrm{EX} + \mathrm{CTPLXA}\ [RhH(PH_3)_3 \rightarrow CO_2] + \mathrm{CTPLXB}\ [CO_2 \rightarrow RhH(PH_3)_3] + \mathrm{R} \quad (9)$$

ES is the electrostatic term arising from the coulombic interaction between $[RhH(PH_3)_3]$ and CO_2; EX is the exchange repulsion due to the Pauli exclusion principle; CTPLXA consists of the charge transfer from $[RhH(PH_3)_3]$ to CO_2, the polarization of CO_2, and their coupling terms; CTPLXB consists of the charge transfer from CO_2 to $[RhH(PH_3)_3]$, the polarization of $[RhH(PH_3)_3]$ and their coupling terms; and R is a higher-order coupling term. By definition, a negative value means a stabilization in energy for all these terms. Although this analysis is based on the HF approximation,[23] the bonding in the transition state can be investigated because the activation energy of this insertion reaction is not influenced very much by electron correlation, as will be described below. The IMSPAC program was used for this analysis.[24]

Results and Discussion

Geometries of the Precursor Complex, Transition State and Product.—In many reactions catalysed by transition-metal complexes a substrate first co-ordinates to (or interacts with) the starting complex to form a precursor complex before proceeding to the transition state. In the precursor complex (**2** in Fig. 1) CO_2 is considerably distant from Rh, and both $[RhH(PH_3)_3]$ and CO_2 are little distorted (compare **2** with **1**), suggesting that any interaction between Rh and CO_2 is very weak (see below). These features are also observed in the insertion of CO_2 into the Cu^I–H bond.[25]§ When a substrate strongly co-ordinates to Rh^I the precursor complex is a d^8 five-co-ordinate system. In such a case there are many possible isomers including trigonal-bipyramidal and square-pyramidal structures, and the course of the insertion is very complicated in a trigonal-bipyramidal structure, as has been theoretically investigated for the insertion of ethene into the Rh^I–H bond of $[RhH(CO)_2(PH_3)(C_2H_4)]$.[26] In the present case, however, we do not need to consider a five-co-ordinate trigonal-bipyramidal structure because the interaction between CO_2 and Rh^I is very weak.

In the transition state the C–H distance between $[RhH(PH_3)_3]$ and CO_2 is 1.46 Å, the Rh–H distance is lengthened only by 0.12 Å and the H ligand barely moves downward from the RhP_3 plane (see transition state in Fig. 1).¶ These geometrical features are common to the insertion reactions of

* The HF optimization with basis set I gives reasonable geometries: $[Rh(OCO_2H)(CO)(PH_3)_2]$ *R*(Rh–O) 2.009 (2.075), *R*(Rh–P) 2.338 (2.333), *R*(Rh–CO) 1.826 (1.798); $[RhH_2(O_2COH)(PH_3)_2]$ *R*(Rh–O) 2.237, 2.239 (2.279, 2.306), *R*(Rh–P) 2.306 (2.302), *R*(Rh–H) 1.512 and 1.513 (1.41 and 1.47) Å, where the values in parentheses are experimental values for $[Rh(OCO_2H)(CO)(PPh_3)_2]$[17a] and $[RhH_2(O_2COH)(PPr^i_3)_2]$.[17b]

† Phosphane is considered as a model of PMe_3.[19] This means that the results presented here are meaningful for the reaction system including non-bulky phosphines.

‡ Eigenvalues of the instability matrix are 0.05, 0.013 and 0.016 for the reactant, transition state and product, when basis set IV is used. The E_a and E_{exo} values calculated at the CCD level are very similar to those calculated at the SDCI levels (Table 3).

§ In the precursor complex, $CuH(PH_3)_2 \cdots CO_2$, the Cu···O^1 distance is 3.28 Å, C···H is 2.66 Å, C–O^1 and C–O^2 are 1.168 and 1.159 Å, the O–C–O angle is 172°, and the Cu–H distance lengthens by 0.06 Å.[25]

¶ The geometry of the reaction system $RhH(PH_3)_3 \cdots CO_2$ was optimized by taking the C–H distance as the reaction coordinate [*R*(C–H) = 1.558, 1.458 (transition state at the HF level), 1.358, 1.308 and 1.258 Å], and then CCD calculations were carried out on these optimized geometries. The transition state was roughly determined at *R*(C–H) = 1.35 Å from the least-squares fitting of CCD total energies. This C–H distance is 0.1 Å longer than the HF-optimized transition-state geometry, but E_a (16.9 kcal mol^{-1}) for this geometry is very similar to that (15.9 kcal mol^{-1}) for the HF-optimized geometry, where E_a are calculated with the CCD/basis set IV method. These results suggest that HF optimization of the transition state followed by single-point correlated calculation seems to provide a reasonable E_a value, while the HF optimization on its own provides a slightly more reactant-like transition state.

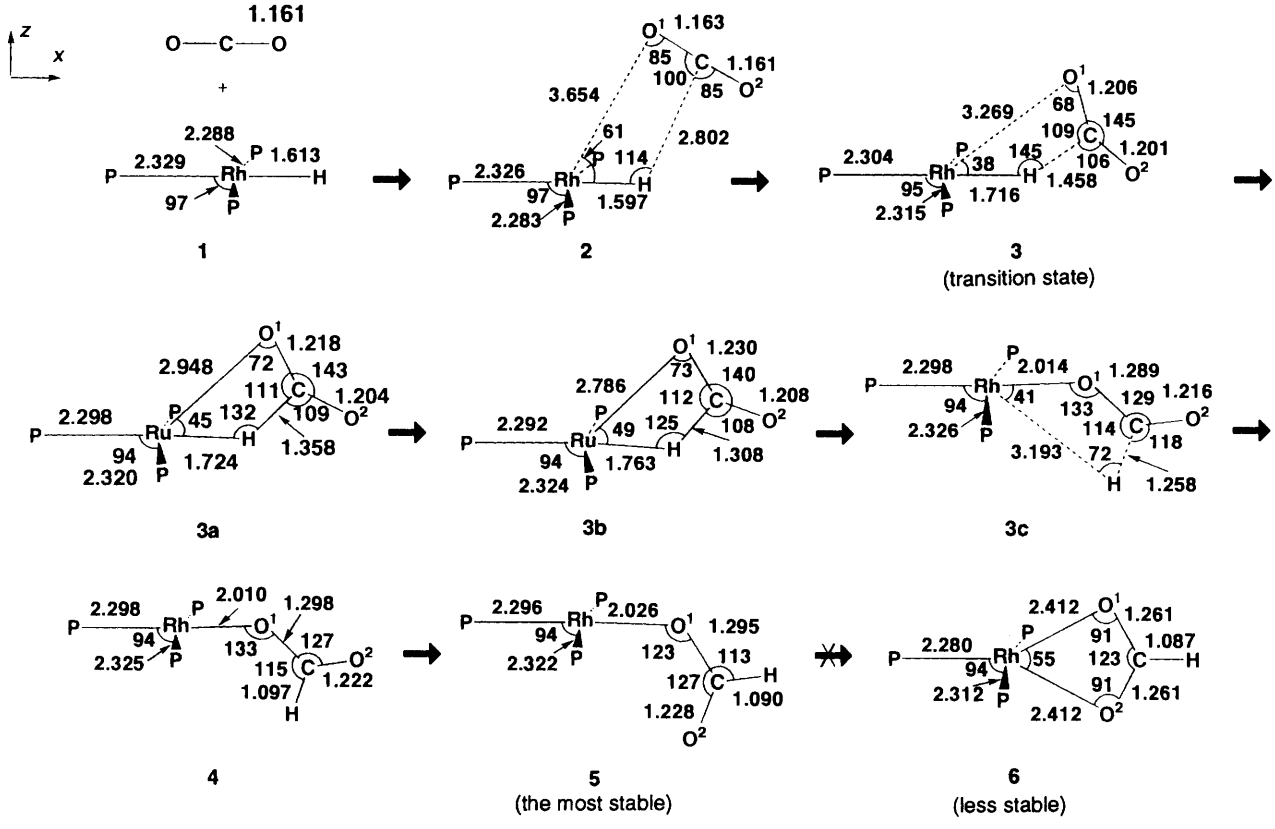

Fig. 1 Geometry changes upon insertion of CO_2 into the Rh^I–H bond of $[RhH(PH_3)_3]$. Bond distances in Å, angles in °. In species **3a**, **3b** and **3c** the geometry was optimized under the assumption that R(C–H) was 1.358, 1.308 and 1.258 Å respectively

Table 1 Basis set effects on the activation energy (E_a) and the exothermicity (E_{exo}) (kcal mol^{-1}) at the HF level for the insertion of CO_2 into the Rh^I–H bond of $[RhH(PH_3)_3]$

	Basis set				
	I	II	III	IV	V
E_a[a]	9.3	14.3	13.3	12.2	11.2
E_{exo}[b]	42.5	37.3	34.9	37.3	38.2

[a] $E_a = E_t$(transition state) − E_t(precursor, **2**). [b] $E_{exo} = E_t$ (**1** + CO_2) − E_t (**5**).

CO_2 into Rh^I–H and Cu^I–H bonds.[3b,25,*] Interesting differences are, however, observed between them; the C–H distance (1.46 Å) between CO_2 and $[RhH(PH_3)_3]$ is shorter than that (1.68 Å) of the copper reaction system, indicating that the transition state of the rhodium system is more product-like. Nevertheless, the Rh^I–O^1 distance (3.27 Å) is much longer than Cu^I–O^1 (2.50 Å), and the Rh–H–C angle (145°) is much larger than Cu–H–C (105°). The C–O^1 distance (1.21 Å) is almost equal to C–O^2 (1.20 Å) in the rhodium system, while C–O^1 (1.21 Å) is longer than C–O^2 (1.18 Å) in the copper system. These differences indicate that the Cu–O^1 bond is partially formed but the Rh–O^1 bond is not yet formed in the transition state. It can, therefore, be reasonably concluded that a four-centre type interaction is hardly involved in the transition state of the rhodium reaction system, but is involved in the copper system.[3b]

Geometry changes after the transition state were then examined, shortening the C–H distance between CO_2 and $[RhH(PH_3)_3]$ to 1.358, 1.308 and 1.258 Å, where the reaction system is becoming similar to the product **4** (see **3a**–**3c** in Fig. 1). This geometry change suggests that although a four-centre type interaction is not formed in the transition state, the product of insertion of CO_2 is Rh[OC(O)H].

For the product there are three possible structures, as shown in Fig. 1: **4** and **5** include a monodentate formate ligand and **6** a bidentate formate ligand. Of them, **5** is the most stable, as will be discussed below.

Recently CO_2 was shown[6] to react with the five-co-ordinate rhodium(I) complexes $[RhH(L\text{–}L)_2]$ (L–L = $Ph_2P(CH_2)_n$-PPh_2, n = 2 or 3), in dimethyl sulfoxide, affording not a Rh[OC(O)H] species but $[Rh(L\text{–}L)_2][HCO_2]$ in which formate exists as a counter anion [equation (2)]. This experimental result is consistent with the geometrical features of the transition state presented here; because the Rh–O^1 bond is hardly formed in the transition state, the insertion of CO_2 into the Rh^I–H bond would not always yield a Rh[OC(O)H] species but yield a free formate anion when co-ordinating species (co-ordinating solvent, four phosphine ligands per Rh, *etc.*) exist in the reaction system.

Activation Energy (E_a) *and Exothermicity* (E_{exo}).—Prior to a detailed discussion of E_a and E_{exo}, the basis-set effects on E_a and E_{exo} will be mentioned here, where E_a is defined as the energy difference between the transition state and the precursor complex **2**, and E_{exo} that between the final product **5** and the sum of reactants, **1** + CO_2. As shown in Table 1, basis set I yields a smaller E_a value and a larger E_{exo} value than do the others. On the other hand, basis set II yields the larger E_a value (note ECP1 was employed in both I and II). Recently, use

* The transition-state structure was roughly determined in our previous work [3b] and correctly optimized at the HF level with the energy-gradient technique in our recent work.[25] The basis sets used for ligand atoms were the same as those in basis set I, and the basis set and ECPs used for Cu were of the same quality as those used for Rh in I (see ref. 3). The Cu–O^1 distance is 2.50 Å, the Cu–H–C angle is 105°, O–C–O is 149°, C–O^1 and C–O^2 are 1.21 and 1.18 Å, respectively, and Cu–H is 1.68 Å {about 0.15 Å longer than in $[CuH(PH_3)_2]$}.

Table 2 Electron-correlation effects on energy changes[a] for insertion of CO_2 into a Rh^I–H bond (kcal mol^{-1})

Species	HF	MP2	MP3	MP4DQ	MP4SDQ	SDCI(DS)[b]	SDCI(P)[c]
1[d] $[RhH(PH_3)_3] + CO_2$	0.0[e]	0.0[f]	0.0[g]	0.0[h]	0.0[i]	0.0[j]	0.0[k]
2 Precursor complex	−1.6	−3.3	−3.3	−3.1	−3.2	−3.4	−3.3
3 Transition state	11.7	14.8	9.8	13.5	12.4	12.8	12.8
	(13.3)[l]	(18.1)	(13.1)	(16.6)	(15.6)	(16.2)	(16.1)
4 $[Rh\{OC(O)H\}(PH_3)_3]$	−29.0	−1.0	−20.1	−11.3	−9.7	−16.2	−16.5
5	−34.9	−6.7	−25.9	−17.0	−15.3	−22.0	−22.4
6 $[Rh(O_2CH)(PH_3)_3]$	−21.7	2.5	−15.4	−6.8	−6.3	—	—

[a] Basis set III was used. [b] Correction by Davidson and Silver for higher-order excitations. [c] Correction by Pople *et al.*[21] for higher-order excitations. [d] See Fig. 1 for these numbers. [e] $E_t(HF) = -1322.6328E_h$. [f] $E_t(MP2) = -1323.3920E_h$. [g] $E_t(MP3) = -1323.3619E_h$. [h] $E_t(MP4DQ) = -1323.4118E_h$. [i] $E_t(MP4SDQ) = -1323.4400E_h$. [j] $E_t[SDCI(DS)] = -1323.4231E_h$. [k] $E_t[SDCI(P)] = -1323.4118E_h$. [l] The energy difference between species **2** and **3**, which corresponds to the activation energy, is given in parentheses.

Table 3 Stabilization energy of the precursor complex E_{stab}, activation energy E_a, and exothermicity E_{exo} for the insertion of CO_2 into Rh^I–H and Cu^I–H bonds (kcal mol^{-1})[a]

	$[RhH(PH_3)_3]$			$[CuH(PH_3)_2]$[b]		
	E_{stab}	E_a[c]	E_{exo}[c]	E_{stab}	E_a[c]	E_{exo}[c]
HF	1.5	12.2	37.3	3.5	3.7	51.4
MP4DQ	3.2	21.0	17.8	4.5	5.9	43.6
MP4SDQ	3.2	20.5	15.6	4.4	7.1	40.1
SDCI(DS)	3.5	15.7	24.0	5.0	3.5	39.4
SDCI(P)	3.5	15.6	24.2	5.0	3.6	39.7
CCD[d]	3.1	15.9	18.7	—	—	—

[a] The bsis set IV was used. E_t of $[RhH(PH_3)_3] + CO_2$ is -5896.1584 at HF, -5896.9380 at MP4DQ, -5896.9676 at MP4SDQ, -5896.9066 at SDCI(DS), -5896.8954 at SDCI(P) and $-5898.9824E_h$ at CCD; E_t of $[CuH(PH_3)_2] + CO_2$ is -2509.2300 at HF, -2510.0240 at MP4DQ, -2510.0713 at MP4DQ, -2510.0162 at SDCI(DS) and $-2510.0057E_h$ at SDCI(P). [b] The E_a and E_{exo} values for the copper system were calculated at the SDCI level, using basis set IV, where geometries were optimized in our previous work.[3b,25] [c] See footnotes *a* and *b* of Table 1 for definitions. [d] The contribution of singly and triply excited configurations is evaluated through doubly excited configurations.

of ECP2 has been recommended for calculating energy changes.[27,28] Also in our calculations of the insertion of CO_2 into the Cu^I–R bond[25] basis set II yielded a much different E_{exo} value from that calculated with III. Thus, it is necessary to use basis set III or a better one in investigating the insertion of CO_2 into the Rh^I–H bond. In the present work, basis set IV was mainly used, except that III was employed for comparing several computational methods at the correlated level.

We now examine the electron-correlation effects on E_a and the energy of the reaction (ΔE). As clearly seen from Table 2, the introduction of electron correlation somewhat increases E_a but considerably decreases the exothermicity (a negative value of ΔE indicates exothermicity). Thus, introduction of electron correlation is indispensable for quantitative estimation of E_a and ΔE. The other important result is that MP2 and MP3 methods are not reliable for investigating the CO_2 insertion, because E_a and ΔE significantly fluctuate. On the other hand, MP4DQ, MP4SDQ and SDCI calculations yield similar E_a values, while the ΔE values at the SDCI level are a little bit larger than those at the MP4SDQ level. In Table 3 we can also see that SDCI and CCD calculations yield almost the same E_a value and that the E_{exo} value calculated at the CCD level is intermediate between those at the MP4SDQ and SDCI levels. Thus, a method of higher quality than that of MP4 should be applied in the present study. The SDCI method was mainly used in comparing the rhodium and copper reaction systems.

As seen in Table 3, the stabilization energy of the precursor complex is very small at all computation levels adopted. This small stabilization energy is consistent with the long Rh···CO_2 distance and the very small distortion of the $[RhH(PH_3)_3]$ and CO_2 constituents (see below). This is not surprising because co-ordination bonds of CO_2 to transition metals are, in general, weak. The activation energy was calculated to be *ca.* 12 kcal mol^{-1} at the HF level and *ca.* 16 kcal mol^{-1} at the SDCI level (after correction for higher-order excited configurations). This activation energy is considerably higher than that for insertion of CO_2 into the Cu^I–H bond (3.5 kcal mol^{-1}).

Before discussing the energy of the reaction, we must examine the relative stabilities of the products. As shown in Table 2, **5** is the most stable, **4** the next and **6** is the least stable at the HF, MP2–MP4SDQ and SDCI levels. These relative stabilities differ from those of the products of insertion of CO_2 into the Cu^I–H bond of $[CuH(PH_3)_2]$. This difference is easily interpreted in terms of the electron configurations of Rh^I and Cu^I; the former prefers a four-co-ordinate square-planar structure **5** to a five-co-ordinate pseudo-trigonal-bipyramidal structure **6** due to its d^8 electron configuration, whereas the latter prefers a four-co-ordinate pseudo-tetrahedral structure due to its d^{10} electron configuration. In the insertion of CO_2 into the Rh^I–Ph bond of $[RhPh(PR_3)_3]$[5] the formate-*O*-species is formed first and then converted into the formate-*O*,*O*′-species after one PR_3 ligand dissociates from Rh [equation (1)].[5] Our calculation is consistent with this experimental result.

For the rhodium system, the exothermicity is calculated to be 24 kcal mol^{-1} at the SDCI level and 19 kcal mol^{-1} at the CCD level (Table 3). This is much smaller than that for insertion of CO_2 into the Cu^I–H bond (*ca.* 40 kcal mol^{-1}).[3b] Comparing the E_a and E_{exo} values, we can conclude that insertion of CO_2 into the Rh^I–H bond occurs less easily than into the Cu^I–H bond of $[CuH(PH_3)_2]$.

Electron Redistribution upon Insertion and Bonding Interactions in the Transition State.—Changes in Mulliken populations are shown in Fig. 2, in which several interesting features are observed. (1) The electron population of CO_2 considerably increases, while those of Rh and Cu remarkably decrease, indicating that the charge transfer from $[RhH(PH_3)_3]$ to CO_2 is important in the insertion. (2) The populations of O^1 and O^2 increase more than that of C in both systems. This electron redistribution arises from mixing of the π orbital of CO_2 with the bonding overlap between the π^* orbital of CO_2 and the highest occupied molecular orbital (HOMO) of $[RhH(PH_3)_3]$. This kind of orbital mixing is in general observed in transition-metal complexes of CO_2 and their reactions. A detailed explanation has been presented previously.[3,29] (3) In the rhodium system the hydrogen population increases in the transition state unexpectedly. Since the electron population of CO_2 also considerably increases, this increase cannot be attributed to charge transfer from CO_2 to $[RhH(PH_3)_3]$. One plausible explanation is that the $\delta+$ charge on the C atom of CO_2 causes polarization of $[RhH(PH_3)_3]$ by which electrons are accumulated on the H ligand so strengthening the $C^{\delta+}$ ··· $H^{\delta-}$ coulombic interaction between CO_2 and $[RhH(PH_3)_3]$. In the copper system, on the other hand, the hydrogen

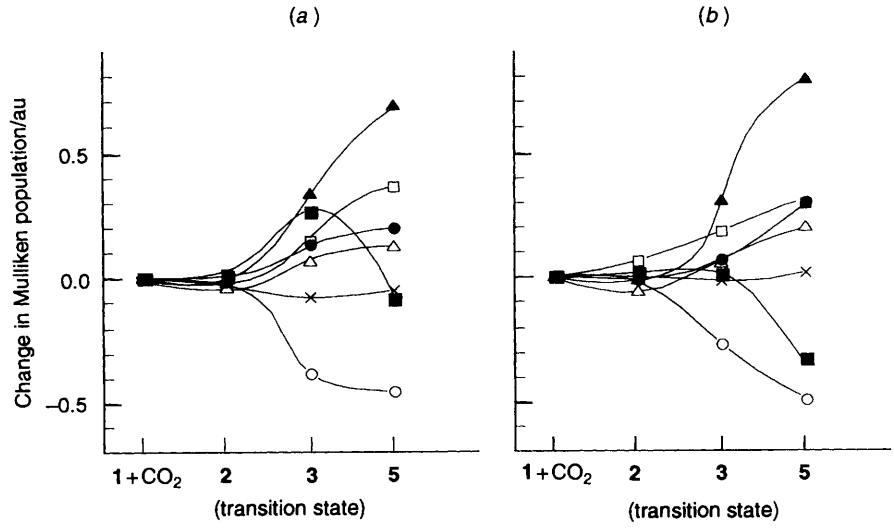

Fig. 2 Changes in Mulliken population upon insertion of CO_2 into a Rh^I–H (*a*) or Cu^I–H (*b*). A positive value means an increase in population. The infinite separation between CO_2 and $[RhH(PH_3)_3]$ is taken to be the standard (change 0). Basis set IV was used. In (*a*) the average value for the three PH_3 ligands was employed. ▲, CO_2; □, O^1; ●, O^2; △, C; ■, H; ×, PH_3; ○, M (Rh or Cu)

Table 4 Energy decomposition analysis (kcal mol^{-1}) of an interaction between CO_2 and $MH(PH_3)_n$ (M = Cu or Rh, n = 2 or 3) in the transition state

	$RhH(PH_3)_3 \cdots CO_2$		$CuH(PH_3)_2 \cdots CO_2$	
	θ 145 (transition state)	106°[b]	145[b]	106° (transition state)
ΔE	10.6	23.1 (19.2)[c]	5.1	0.4
DEF total	25.7	25.7 (25.7)	21.7	21.7
$[MH(PH_3)_n]$	0.8	0.8 (0.8)	2.1	2.1
CO_2	24.9	24.9 (24.9)	19.6	19.6
INT	−15.1	−2.6 (−6.5)	−16.6	−21.3
ES	−55.9	−103.6 (−63.0)	−47.5	−71.0
EX	106.5	189.3 (105.7)	70.5	101.7
CTPLXA $\{[MH(PH_3)_n] \rightarrow CO_2\}$	−44.7	−59.3 (−35.2)	−28.6	−37.9
CTPLXB $\{CO_2 \rightarrow [MH(PH_3)_n]\}$	−13.8	−20.7 (−10.8)	−7.4	−8.9
R	−7.2	−8.4 (−3.2)	−3.6	−5.2

[a] The basis set IV was used. A positive value means destabilization in energy (and *vice versa*). [b] Only the angle θ (M–H–C) is changed, the remaining geometry being unchanged. [c] In parentheses are given the values corresponding to an increase in the C–H distance between CO_2 and $[RhH(PH)_3)_3]$ to 1.678 Å which is that in the transition state of the copper system.

Table 5 Partitioning of population changes* in the transition state

	$[RhH(PH_3)_3]$				$[CuH(PH_3)_2]$			
	Rh	H	PH_3(av)	CO_2	Cu	H	PH_3	CO_2
EX	0.013	−0.024	0.008	0.0	−0.014	0.013	0.001	0.0
CTPLXA	−0.152	−0.134	−0.014	0.329	−0.140	−0.163	0.0	0.303
CTPLXB	−0.425	0.476	−0.045	−0.023	−0.170	0.198	0.008	−0.038

* Difference from the population at infinite separation between CO_2 and $[MH(PH_3)_n]$ (M = Cu or Rh, n = 2 or 3). A positive value means an increase in population (and *vice versa*).

population hardly increases in the transition state [Fig. 2(*b*)]. This difference suggests that $[RhH(PH_3)_3]$ is much more polarizable than is $[CuH(PH_3)_2]$, as will be discussed below in more detail.

To inspect the bonding interaction in the transition state an energy decomposition analysis was performed, as shown in Tables 4 and 5. The ES stabilization cannot counterbalance the EX repulsion, as is often found in the reactions of transition-metal complexes.[3b,30] This means that the static interaction, which corresponds to the sum of ES and EX, is repulsive and the contribution from the CTPLXA and CTPLXB terms is necessary to stabilize the transition state of the insertion reaction. The CTPLXA term yields much greater stabilization than does CTPLXB. This result is consistent with the electron redistribution discussed above, since the main contribution to the CTPLXA term is charge transfer from $[RhH(PH_3)_3]$ to CO_2. The electron population of CO_2 increases, but those of Rh and H decrease, through this term (Table 5). Although the CTPLXB stabilization is small, its contribution cannot be neglected. The electron population of CO_2 is slightly decreased, that of Rh is considerably decreased but that of H is remarkably increased by this term (Table 5). These results indicate that the charge transfer from CO_2 to $[RhH(PH_3)_3]$ does not contribute very much to the CTPLXB term but the polarization of

$[RhH(PH_3)_3]$ does considerably. In the copper system the hydrogen population increases through this term to a much lesser extent than in the rhodium system (Table 5). This is because $[CuH(PH_3)_2]$ is much less polarizable than is $[RhH(PH_3)_3]$. The increase in the hydrogen atomic population through the CTPLXB term is almost compensated by its decrease through the CTPLXA term (Table 5). Thus, the population hardly changes in the transition state of the copper system [Fig. 2(*b*)].

Differences between $[RhH(PH_3)_3]$ *and* $[CuH(PH_3)_2]$ *in the Insertion Reaction.*—One of the great differences between these two reaction systems is that insertion of CO_2 into the Rh^I–H bond is much less exothermic than that into the Cu^I–H bond (Table 3). The exothermicity is mainly determined by bond energies. In the course of insertion the M–H bond is broken, while M–OC(O)H and H–C(O)OM bonds are formed. The formation of the H–C(O)OM bond is common to both systems. Thus, the difference in exothermicity mainly arises from the Rh^I–H, Cu^I–H, Rh^I–OC(O)H and Cu^I–OC(O)H bond energies. Considering equation (10), we can estimate the difference

$$[Rh(PH_3)_3]^+ + [CuH(PH_3)_2] \longrightarrow [RhH(PH_3)_3] + [Cu(PH_3)_2]^+ \quad (10)$$

between the Rh^I–H and Cu^I–H bond energies, as shown in equation (11) where $\Delta E_{r-1} = E_t$ (right-hand side) $- E_t$ (left-

$$\Delta E_{r-1} = E(Cu\text{–}H) + E(Rh\text{–}H) \quad (11)$$

hand side). Similarly, we can estimate the difference between the Rh^I–OC(O)H and Cu^I–OC(O)H bond energies from equations (12) and (13) where the geometries of $[Cu(PH_3)_2]^+$

$$[Rh(PH_3)_3]^+ + [Cu\{OC(O)H\}(PH_3)_2] \longrightarrow [Rh\{OC(O)H\}(PH_3)_2] + [Cu(PH_3)_2]^+ \quad (12)$$

$$\Delta E_{r-1} = E[Cu\text{–}OC(O)H] - E[Rh\text{–}OC(O)H] \quad (13)$$

and $[Rh(PH_3)_3]^+$ were optimized at the HF level, using the basis set I. As shown in Table 6, E(Rh–H) is 28–31 kcal mol^{-1} larger than E(Cu–H) at the MP4 level, while E[Rh–OC(O)H] is only 6–7 kcal mol^{-1} larger than E[Cu–OC(O)H]. In the rhodium system, therefore, the considerably stronger Rh–H bond is broken but an only slightly stronger Rh–OC(O)H bond is formed compared to those in the copper system, which leads to the smaller exothermicity of the rhodium compared to the copper system.

It should be also noted that the rhodium system requires a higher activation energy than that of the copper system. The interaction between CO_2 and $MH(PH_3)_n$ (M = Cu or Rh, n = 2 or 3) in the transition state was investigated by energy decomposition analysis (EDA), which was performed at θ (the M–H–C angle) = 145 and 105°, for M = Rh or Cu. A clear reason for the higher activation energy of the rhodium system can not, however, be found by comparing the two systems at the same θ value, because the rhodium system suffers greater destabilization from DEF and EX terms and greater stabilization from ES, CTPLXA and CTPLXB terms than does the copper system (Table 4). To examine the differences between the two systems, we carried out further EDA of the rhodium system where the C–H distance and the Rh–H–C angle were taken to be the same as those of the copper system (results given in parentheses in Table 4). On comparing this assumed structure with that of the transition state of the copper system, it is seen that the former suffers larger destabilization energies from the DEF and EX terms and receives a smaller stabilization energy from the ES term than does the copper system. Thus, the higher activation energy of the rhodium system can be attributed to the larger DEF value, the smaller ES stabilization

Table 6 Differences in bond energies (kcal mol^{-1}) between Rh^I–X and Cu^I–X [X = H or OC(O)H] *

	E(Rh–H) − E(Cu–H)	E[Rh–OC(O)H]− E[Cu–OC(O)H]
MP2	37.2	9.2
MP3	29.6	8.1
MP4DQ	30.7	6.9
MP4SDQ	28.3	5.5

* The basis set IV was used.

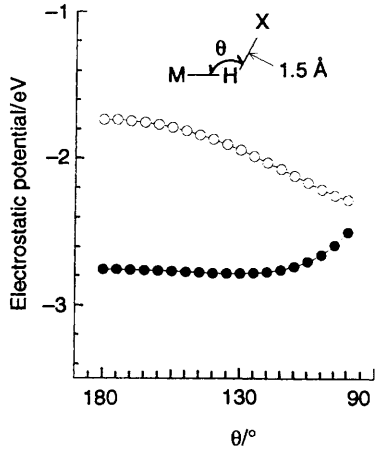

Fig. 3 Electrostatic potentials of $[RhH(PH_3)_3]$ (○) and $[CuH(PH_3)_2]$ (●). A positive value means destabilization of a positive charge. The basis set IV was used

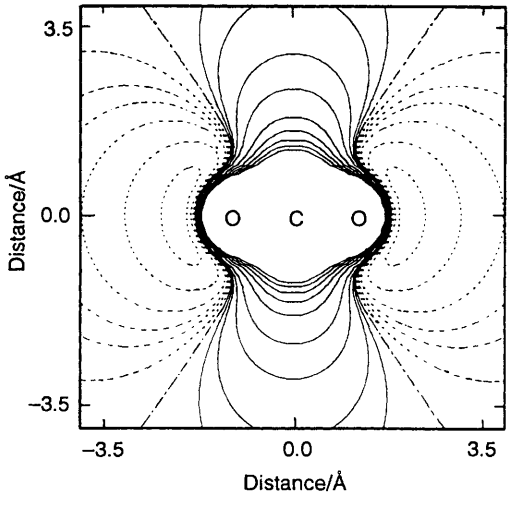

Fig. 4 Map of the electrostatic potential of CO_2. The basis set IV was used. Contour values (in eV) are 0.0, ±0.05, ±0.10, ±0.15, ±0.25, ±0.5, ±1.0, ±1.5, ±2.0, ±2.5 and ±3.0. The solid lines indicate positive values, the dotted lines negative values, and — · — the value of 0.0

and the larger EX repulsion. The large DEF value is due to the large distortion of the CO_2 part (Table 4). In order to break the strong Rh^I–H bond, CO_2 more strongly interacts with the H ligand in the transition state of the rhodium system than it does in the copper system, which results in a larger distortion of the CO_2 part in the former (Fig. 1). Thus, the large DEF value of the rhodium system is related to the strong Rh^I–H bond. The smaller ES stabilization is interpreted in terms of the electrostatic potential. The electrostatic potentials of $[RhH(PH_3)_3]$ and $[CuH(PH_3)_2]$ are compared at a position 1.5 Å distant from the H ligand (Fig. 3). At both θ = 105 and 145°, the electrostatic potential of $[CuH(PH_3)_2]$ is more negative than that of $[RhH(PH_3)_3]$, probably because the H

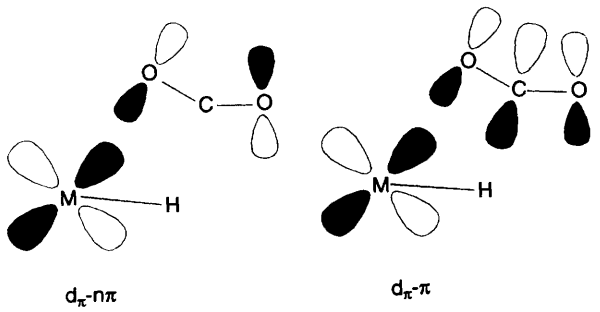

Scheme 1

ligand is more negatively charged in the former (−0.161 e) than in the latter (−0.043 e). Since CO_2 exhibits a positive electrostatic potential toward the H ligand (Fig. 4), the copper system can receive a larger ES stabilization than can the rhodium system. The greater EX repulsion of the rhodium system can be understood by considering the occupied $4d_{xz}$ orbital of Rh. In general, the 4d orbital expands to a greater extent than does the 3d orbital, and furthermore the Cu atom possesses the least expanding 3d orbital of the elements in the first transition series. Thus, the rhodium $4d_{xz}$ orbital gives rise to larger EX repulsion with the π and nπ orbitals of CO_2 than does copper $3d_{xz}$ orbital (Scheme 1). These results lead to the conclusion that the higher activation energy of the rhodium system arises from the stronger Rh^I–H bond, the smaller electrostatic potential of $[RhH(PH_3)_3]$, and the more expansible $4d_{xz}$ orbital of Rh than those of $[CuH(PH_3)_2]$.

There are outstanding differences in the transition-state structure between the two reaction systems. The first is that the C–H distance between CO_2 and the H ligand is much shorter in the rhodium system than in the copper system (Fig. 1). This is because CO_2 must interact strongly with the H ligand to break the strong Rh^I–H bond (see above). The next is that the Rh–H–C angle is much larger than Cu–H–C (see above). As clearly shown in Table 4, both destabilization from the EX term and stabilization from the ES and CTPLXA terms increase as θ decreases. The increase in EX repulsion energy cannot be overcome by the increases in ES and CTPLXA stabilization energies in the rhodium system, but can be in the copper system. This difference is easily explained, as follows. The decrease in θ enlarges the overlap of the rhodium $4d_{xz}$ orbital with the π and nπ orbitals of CO_2 (Scheme 1), which increases the EX repulsion between them. Owing to the smaller expanse of the copper 3d orbital (see above), the EX repulsion is intrinsically weak in the copper system. Thus, the decrease in θ strengthens the exchange repulsion of this system to a lesser extent than that of the rhodium system. Accordingly, θ is large in the transition state of the rhodium system but small in the copper system. Although the dependences of the ES and CTPLXA terms on the angle θ can be explained in terms of the electrostatic potential and the expanse of the d_{xz} orbital, we leave the explanation here, because these dependences are not the main point of discussion.

Conclusion

The insertion of CO_2 into the Rh^I–H bond easily occurs with an activation barrier of *ca.* 16 kcal mol^{-1} and exothermicity of *ca.* 24 kcal mol^{-1} (at the SDCI level), yielding $[Rh\{OC(O)H\}(PH_3)_3]$. This activation barrier is higher and the exothermicity lower than those of the similar insertion into the Cu^I–H bond of $[CuH(PH_3)_2]$ (E_a = 3.5 and E_{exo} = *ca.* 40 kcal mol^{-1} at the SDCI level). The higher activation energy of the rhodium system results from the facts that the Rh^I–H bond is stronger than the Cu^I–H bond, the negative electrostatic potential of $[RhH(PH_3)_3]$ is smaller than that of $[CuH(PH_3)_2]$, and the EX repulsion between CO_2 and $[RhH(PH_3)_3]$ is greater than that between CO_2 and $[CuH(PH_3)_2]$. The lower exothermicity is due to the stronger Rh^I–H bond. The transition state of the rhodium system has a shorter C–H distance between CO_2 and the H ligand than does that of the copper system. The strong Rh^I–H bond is the reason for the short C–H distance; the CO_2 must approach closer to the H ligand so as to break this strong bond. The θ angle in the transition state is much different between the two systems, 145° in the rhodium system but only 105° in the copper system. The larger Rh–H–C angle arises from the strong EX repulsion between the $4d_{xz}$ orbital of Rh and the π and nπ orbitals of CO_2. The rhodium $4d_{xz}$ orbital expands more than does the Cu $3d_{xz}$ orbital, which gives rise to the stronger EX repulsion. From these results we can predict that the insertion of CO_2 into M–H bond occurs easily when this bond is weak, the electrostatic potential of the metal hydride complex is negatively large, and the expanse of the d_π orbital is small.

Acknowledgements

All calculations were carried out with Hitachi S-820 and M-680H computers of the Institute for Molecular Science, Okazaki and an IBM-RS-6000/340 work station of our laboratory. This work was supported in part by a grant from the Ministry of Education, Culture and Science (No. 04243102).

References

1 F. R. Hartley and S. Patai, *The Chemistry Metal–Carbon Bonds*, Wiley, New York, 1985, vol. 3; R. H. Crabtree, *The Organometallic Chemistry of Transition Metals*, Wiley, New York, 1988.
2 D. J. Darensbourg and R. A. Kudaroski, *Adv. Organomet. Chem.*, 1983, **22**, 129; A. Behr, *Angew. Chem., Int. Ed. Engl.*, 1988, **27**, 661.
3 S. Sakaki and K. Ohkubo, (*a*) *Inorg. Chem.*, 1988, **27**, 2020; (*b*) *Inorg. Chem.*, 1989, **28**, 2583; (*c*) *Organometallics*, 1989, **8**, 2970.
4 C. Bo and A. Dedieu, *Inorg. Chem.*, 1989, **28**, 304.
5 D. J. Darensbourg, G. Grötsch, P. Wiegreffe and A. L. Rheingold, *Inorg. Chem.*, 1987, **26**, 3827.
6 T. Burgmemeiser, F. Kastner and W. Leitner, *Angew. Chem., Int. Ed. Engl.*, 1993, **32**, 739.
7 J.-C. Tsai and K. M. Nicholas, *J. Am. Chem. Soc.*, 1992, **114**, 5117.
8 W. C. Kaska, S. Nemeh, A. Shiraze and S. Potunik, *Organometallics*, 1988, **7**, 13.
9 S. H. Strauss, K. H. Whitmire and D. F. Shriver, *J. Organomet. Chem.*, 1979, **174**, C59.
10 M. J. Frisch, J. S. Binkley, H. B. Schlegel, K. Raghavachari, C. F. Melius, R. L. Martin, J. J. P. Stewart, F. W. Bobrowicz, C. M. Rohlfing, L. R. Kahn, D. J. DeFrees, R. Seeger, R. A. Whiteside, D. J. Fox, E. M. Fluder, S. Topiol and J. A. Pople, GAUSSIAN 86, Carnegie-Mellon Quantum Chemistry Publishing Unit, Pittsburgh, PA, 1986.
11 M. J. Frisch, G. W. Trucks, M. Head-Gordon, P. M. W. Gill, M. W. Wong, J. B. Foresman, B. G. Johnson, H. B. Schlegel, M. A. Robb, E. S. Replogle, R. Gomperts, J. L. Andres, K. Raghavachari, J. S. Binkley, C. Gonzalez, R. L. Martin, D. J. Fox, D. J. DeFrees, J. Baker, J. J. P. Stewart and J. A. Pople, GAUSSIAN 92, Gaussian Inc., Pittsburgh, PA, 1992.
12 P. J. Hay and W. R. Wadt, *J. Chem. Phys.*, 1985, **82**, 270.
13 S. Huzinaga, J. Andzelm, M. Klobukowski, E. Radzio-Andzelm, Y. Sakai and H. Takewaki, *Gaussian Basis Sets for Molecular Calculations*, Elsevier, Amsterdam, 1984.
14 W. J. Hehre, R. Ditchfield, R. F. Stewart and J. A. Pople, *J. Chem. Phys.*, 1970, **52**, 2769.
15 T. H. Dunning and P. J. Hay, *Methods of Electronic Structure Theory*, ed. H. F. Schaefer, Plenum, New York, 1977, p. 1.
16 P. J. Hay and W. R. Wadt, *J. Chem. Phys.*, 1985, **82**, 299.
17 (*a*) S. F. Hossain and K. M. Nicholas, *J. Chem. Soc., Chem. Commun.*, 1981, 268; (*b*) T. Yoshida, D. L. Thorn, T. Okano, J. A. Ibers and S. Otsuka, *J. Am. Chem. Soc.*, 1979, **101**, 4212.
18 G. Herzberg, *Molecular Spectra and Molecular Structure*, Van Nostrand, Princeton, NJ, 1967, vol. 3, p. 610.
19 J. O. Noell and P. J. Hay, *J. Am. Chem. Soc.*, 1982, **104**, 4578.
20 E. R. Davidson and D. W. Silver, *Chem. Phys. Lett.*, 1977, **52**, 403.
21 J. A. Pople, R. Seeger and R. Krishnan, *Int. J. Quantum. Chem. Symp.*, 1977, **11**, 149.
22 R. Seeger and J. A. Pople, *J. Chem. Phys.*, 1977, **66**, 3045 and refs. therein.

23 K. Morokuma, *Acc. Chem. Res.*, 1977, **10**, 294; K. Kitaura and K. Morokuma, *Int. J. Quantum Chem.*, 1976, **10**, 325; K. Kitaura, S. Sakaki and K. Morokuma, *Inorg. Chem.*, 1981, **20**, 2292.
24 K. Morokuma, S. Kato, K. Kitaura, I. Ohmine, S. Sakai and S. Obara, IMSPACK, IMS Computer Program Library No. 0372, The Institute for Molecular Science, Okazaki, Japan, 1980.
25 S. Sakaki and Y. Musashi, unpublished work.
26 N. Koga, S. Q. Jin and K. Morokuma, *J. Am. Chem. Soc.*, 1988, **110**, 3417.
27 P. J. Hay, *New J. Chem.*, 1991, **15**, 735.
28 T. Leininger, J.-F. Riehl, G.-H. Jeung and M. Pèlissier, *Chem. Phys. Lett.*, 1993, **205**, 301.
29 S. Sakaki, T. Aizawa, N. Koga, K. Morokuma and K. Ohkubo, *Inorg. Chem.*, 1989, **28**, 103; S. Sakaki, *J. Am. Chem. Soc.*, 1992, **114**, 2055.
30 S. Sakaki, K. Maruta and K. Ohkubo, *J. Chem. Soc., Dalton Trans.*, 1987, 361; *Inorg. Chem.*, 1987, **26**, 2499.

Received 5*th January* 1994; *Paper* 4/00044G